Supporting Information

Regulating spin polarization by diatomic doping for NiFe Layered Double Hydroxide to achieve efficient electrocatalytic water splitting

*Hui-Zhan Wen, Zha-Xi Wan-Me, Yang Zhao, Xue-Ying Wan, Hai-Tao Zhang, Yu-Long Xie**

School of Chemistry and Materials Science, Qinghai Minzu University, Key Laboratory of Resource Chemistry and Eco-environmental Protection in Tibetan Plateau of State Ethnic Affairs Commission, Qinghai Provincial Key Laboratory of Nanomaterials and Nanotechnology, Xining, 810007, China

*Corresponding author.

E-mail: yulongxie2012@126.com

1.Supplementary Figures

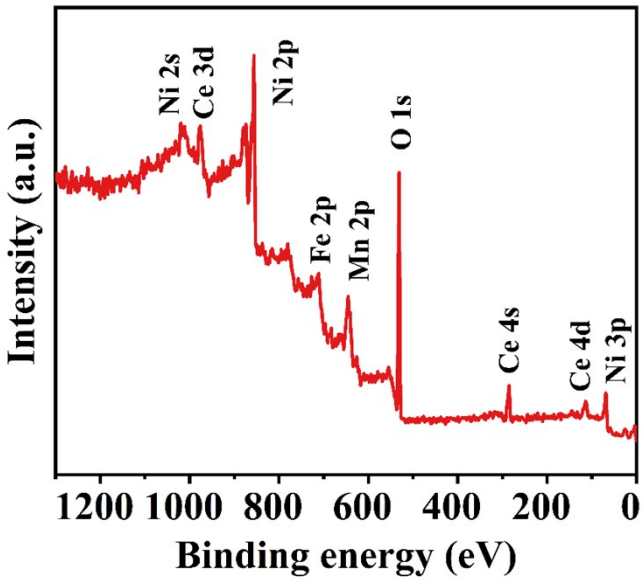

Figure S1 High-resolution XPS full spectrum of $Mn_{0.2}Ce_{0.8}$-NiFe-LDH/NF.

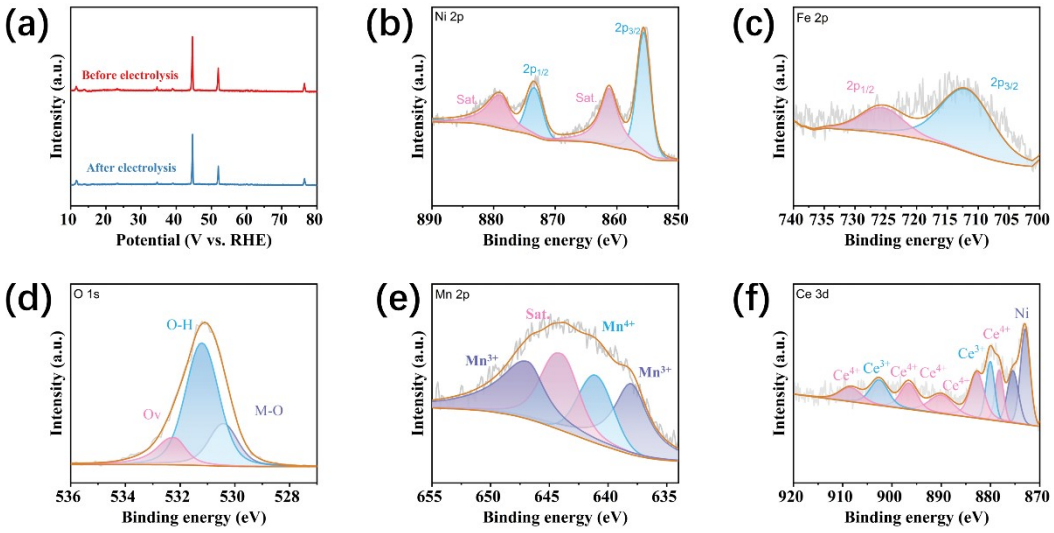

Figure S2 (a) XRD spectra of $Mn_{0.2}Ce_{0.8}$-NiFe-LDH/NF after stability testing, $Mn_{0.2}Ce_{0.8}$-NiFe-LDH/NF with (b) Ni 2p, (c) Fe 2p, (d) O 1s, (e) Mn 2p, (f) Ce 3d high-resolution XPS spectra after stability testing.

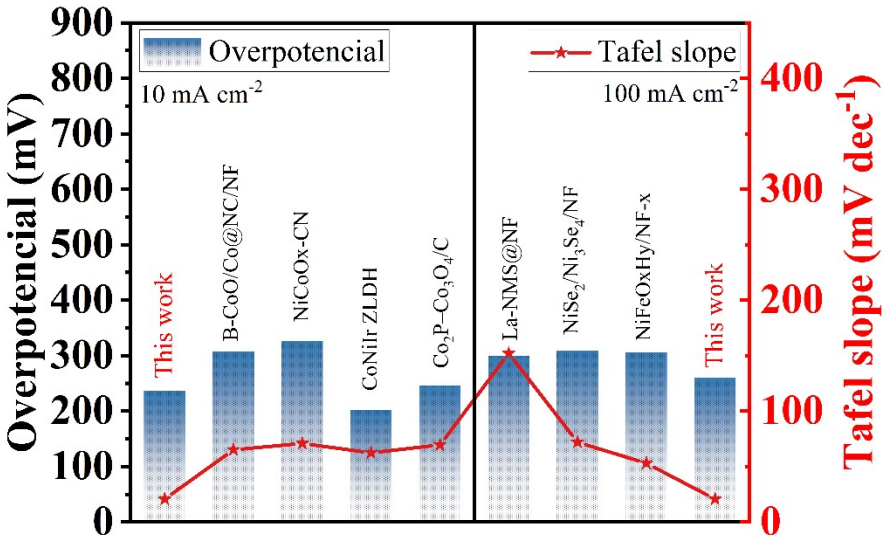

Figure S3 The comparison of OER performance for some representative non-noble electrocatalysts.

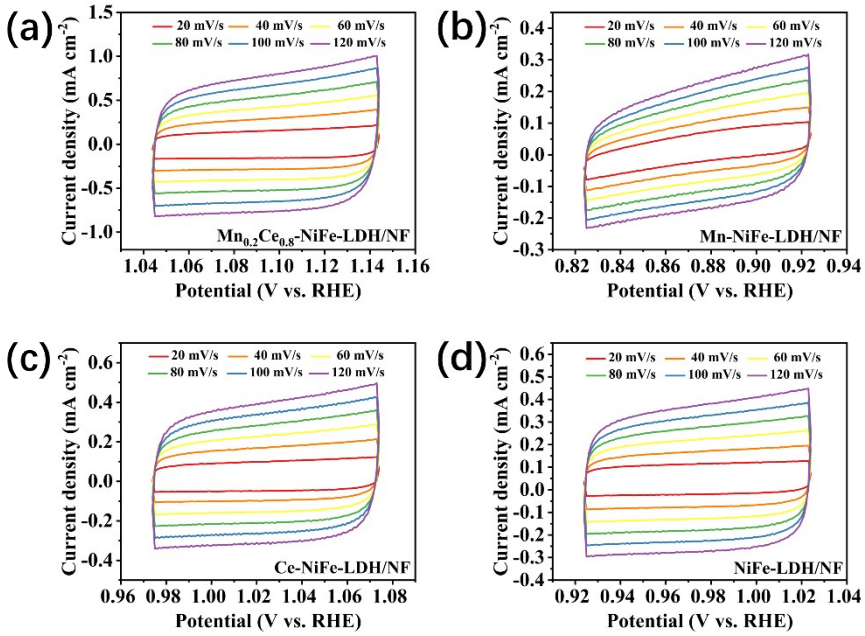

Figure S4 CV curves of (a) $Mn_{0.2}Ce_{0.8}$-NiFe-LDH/NF, (b) Mn-NiFe-LDH/NF, (c) Ce-NiFe-LDH/NF, and (d) NiFe-LDH/NF for the OER reaction at different scan rates.

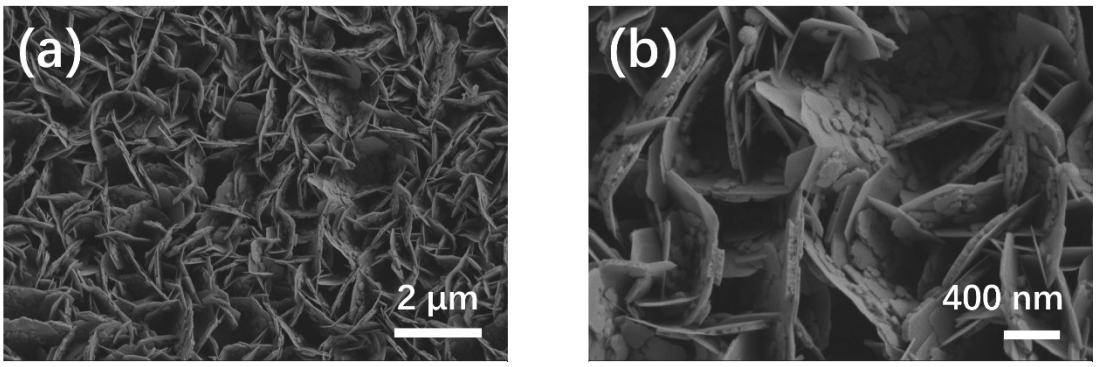

Figure S5 SEM image of $Mn_{0.2}Ce_{0.8}$-NiFe-LDH/NF after OER stability testing(a) 2 μm and (b) 400 nm.

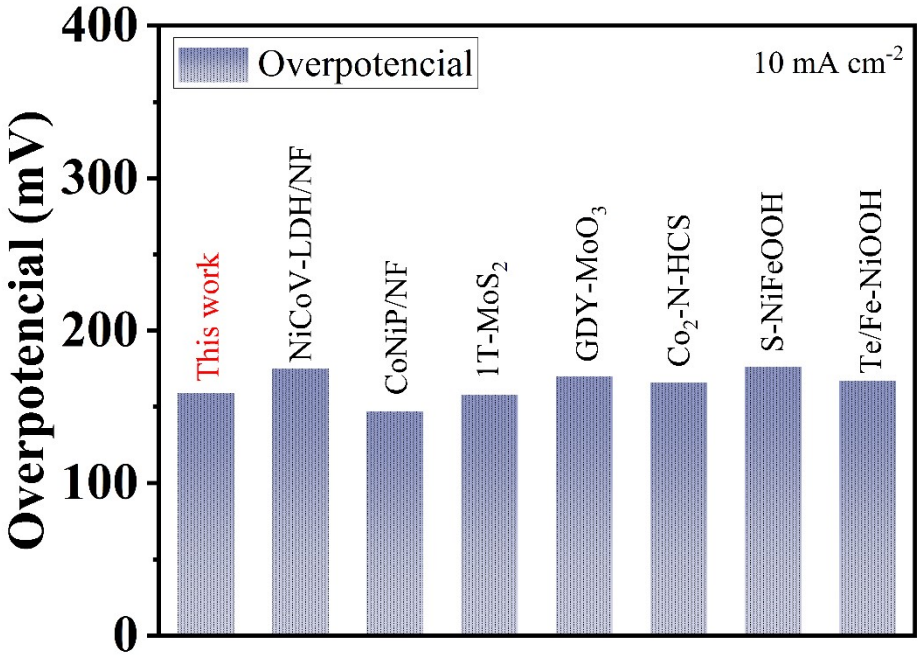

Figure S6 The comparison of HER performance for some representative non-noble electrocatalysts.

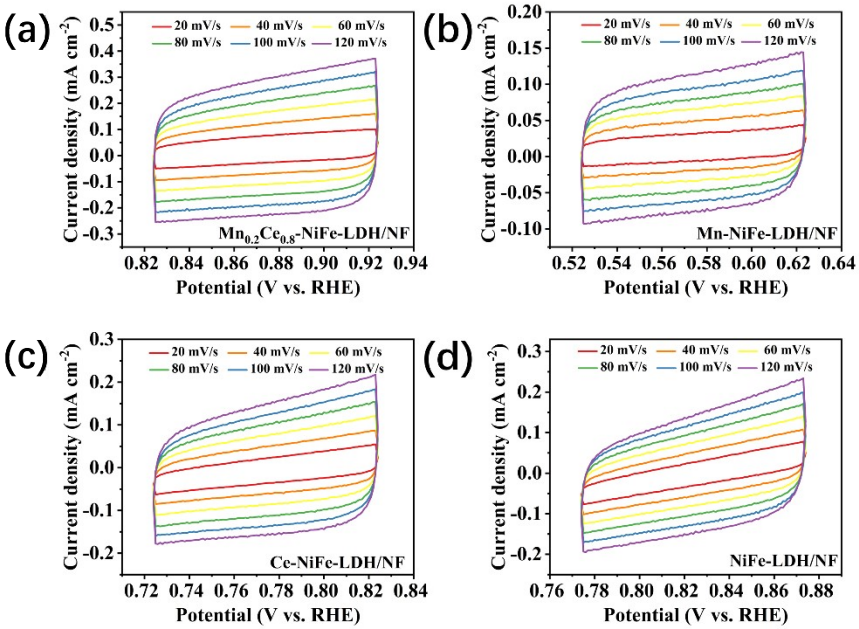

Figure S7 CV curves of (a) $Mn_{0.2}Ce_{0.8}$-NiFe-LDH/NF, (b) Mn-NiFe-LDH/NF, (c) Ce-NiFe-LDH/NF, and (d) NiFe-LDH/NF for the HER reaction at different scan rates.

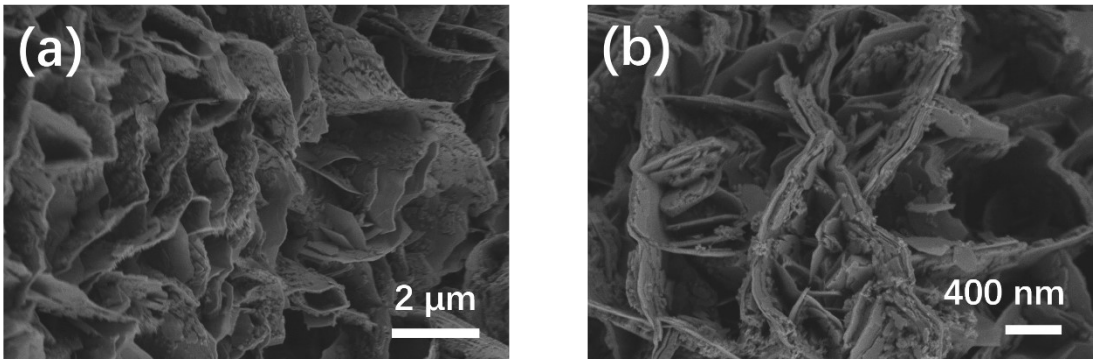

Figure S8 SEM image of $Mn_{0.2}Ce_{0.8}$-NiFe-LDH/NF after HER stability testing(a) 2 μm and (b) 400 nm.

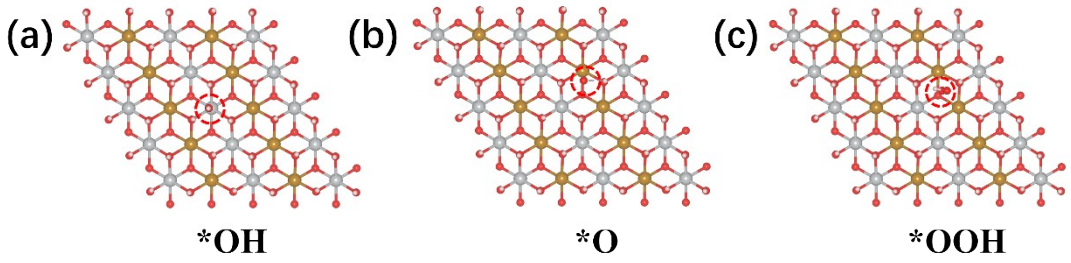

Figure S9 Optimized configurations of intermediates (a)OH*, (b)O* and (c)OOH* of NiFe-LDH/NF

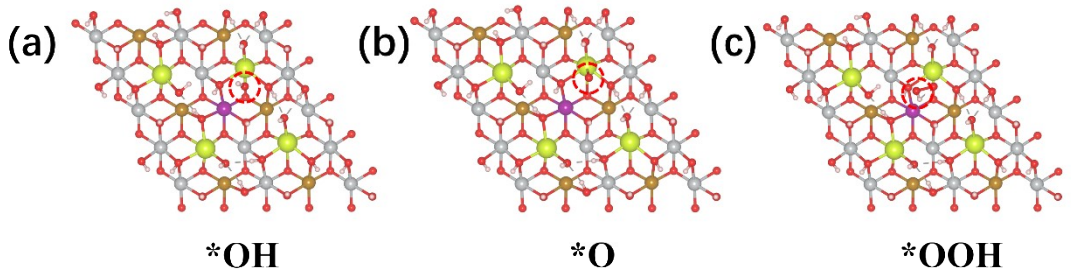

Figure S10 Optimized configurations of intermediates (a)OH*, (b)O* and (c)OOH* of $Mn_{0.2}Ce_{0.8}$-NiFe-LDH/NF

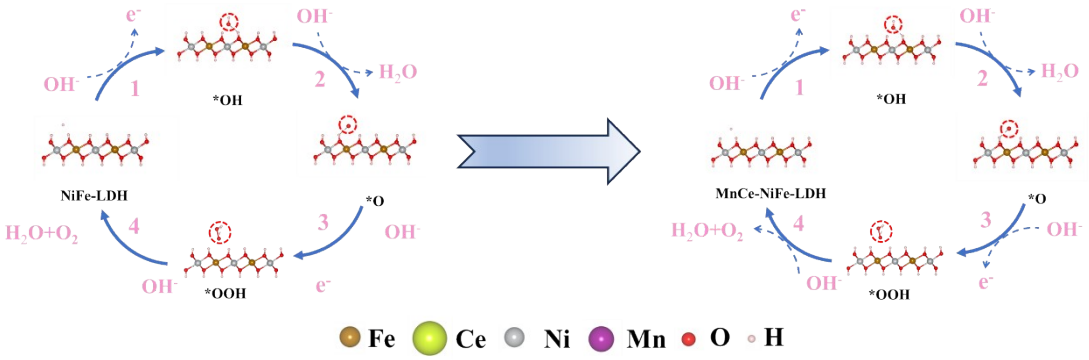

Figure S11 Schematic of the OER mechanism for NiFe-LDH/NF and $Mn_{0.2}Ce_{0.8}$-NiFe-LDH/NF.

2. Supplementary Tables

Table S1 Comparison of electrocatalytic performance for OER to other reported catalysts in 1.0 M KOH.

Catalysts	J ($mA\ cm^{-2}$)	η mV (vs.RHE)	Tafel slope ($mV\ dec^{-1}$)	Electrolyte	reference
$Mn_{0.2}Ce_{0.8}$-NiFe-LDH/NF	**10** **100**	**237** **269**	**20.59**	**1.0 M KOH**	**This work**
B-CoO/Co@NC/NF	10	307	65.2	1.0 M KOH	[1]
NiCoOx-CN	10	326	70.8	1.0 M KOH	[2]
Co_2P–Co_3O_4/C	10	246	69.5	1.0 M KOH	[3]
CoNiIr ZLDH	10	202	62.3	1.0 M KOH	[4]
La-NMS@NF	100	300	152	1.0 M KOH	[5]
NiSe2/Ni3Se4/NF	100	309	71.9	1.0 M KOH	[6]
NiFeOxHy/NF-x	100	306	53	1.0 M KOH	[7]
FeS_2MS/NF	100	314	60	1.0 M KOH	[8]
Ni_3S_2/NiO	100	320	46	1.0 M KOH	[9]
RuO_2	10	370	\	1.0 M KOH	[10]

Table S2 Comparison of electrocatalytic performance for HER to other reported catalysts in 1.0 M KOH.

Catalysts	J/$mA\ cm^{-2}$	η/mV(vs.RHE)	Electrolyte	reference
$Mn_{0.2}Ce_{0.8}$-NiFe-LDH/NF	**10** **50**	**159** **229**	**1.0 M KOH**	**This work**
NiCoV-LDH/NF	10	175	1.0 M KOH	[11]
CoNiP/NF	10	147	1.0 M KOH	[12]
1T-MoS_2	10	158	1.0 M KOH	[13]

GDY-MoO_3	10	170	1.0 M KOH	[14]
Co_2-N-HCS	10	166	1.0 M KOH	[15]
S-NiFeOOH	10	176	1.0 M KOH	[16]
Te/Fe-NiOOH	10	167	1.0 M KOH	[17]
NiFeOOH	10	145	1.0 M KOH	[18]
Pd/$NiFeO_x$	10	180	1.0 M KOH	[19]
Pt/C	10	73	1.0 M KOH	[20]

3. Theoretical model information

All the DFT calculations were conducted based on the Vienna Ab initio Simulation Package (VASP) [21] [22]. The exchange-correlation potential was described by the Perdew−Burke−Ernzerhof (PBE) generalized gradient approach (GGA) [23]. The electron-ion interactions were accounted by the projector augmented wave (PAW) [24]. All DFT calculations were performed with a cut-off energy of 400 eV, and the 2×2×1 Monkhorst-Pack grid k-points were selected to sample the Brillouin zone integration. The energy and force convergence criteria of the self-consistent iteration were set to 10^{-5} eV and -0.05 eV $Å^{-1}$, respectively. DFT-D3 method was used to describe van der Waals (vdW) interactions [25].

The Gibbs free energy changes (ΔG) of the reaction are calculated using the following formula:

$$\Delta G = \Delta E + \Delta \mathrm{ZPE} - T\Delta S + \Delta G_{\mathrm{U}} + \Delta G_{\mathrm{pH}}$$

where ΔE is the electronic energy difference directly obtained from DFT calculations, ΔZPE is the zero-point energy difference, T is the room temperature (298.15 K) and ΔS is the entropy change. $\Delta G_{\mathrm{U}} = -eU$, where U is the applied electrode potential. $\Delta G_{\mathrm{pH}} = k_{\mathrm{B}}T \times \ln 10 \times \mathrm{pH}$, where k_{B} is the Boltzmann constant, and pH value is set to 0.

4. Notes and references

1. Cha, D. C.; Singh, T. I.; Maibam, A.; Kim, T. H.; Nam, D. H.; Babarao, R.; Lee, S., Metal–Organic Framework–Derived Mesoporous B-Doped CoO/Co@ N-Doped Carbon Hybrid 3D Heterostructured Interfaces with Modulated Cobalt Oxidation States for Alkaline Water Splitting. Small 2023, 19 (35), 2301405.
2. Le, T. T.; Sharma, P.; Bora, B. J.; Tran, V. D.; Truong, T. H.; Le, H. C.; Nguyen, P. Q. P., Fueling the future: A comprehensive review of hydrogen energy systems and their challenges. Int. J. Hydrogen Energy 2024, 54, 791-816.
3. Huang, G.; Hu, M.; Xu, X.; Alothman, A. A.; Mushab, M. S. S.; Ma, S.; Shen, P. K.; Zhu, J.; Yamauchi, Y., Optimizing heterointerface of Co2P–Co x O y nanoparticles within a porous carbon network for deciphering superior water splitting. Small Structures 2023, 4 (6), 2200235.
4. Xu, W.; Altaf, Q.; Chen, L.; Zhao, J.; Shang, C.; Peng, X.; Hu, L.; Ma, H.; Wen, J., Ir-Induced Local Charge and Electron-Spin Regulation on CoNi LDH Electrocatalyst for Efficient Oxygen Evolution Reaction. The Journal of Physical Chemistry Letters 2025, 16 (29), 7313-7321.
5. Li, W.; Sun, Z.; Ge, R.; Li, J.; Li, Y.; Cairney, J. M.; Zheng, R.; Li, Y.; Li, S.; Li, Q.; Liu, B., Nanoarchitectonics of La-Doped Ni3S2/MoS2 Hetetostructural Electrocatalysts for Water Electrolysis. 2023, 4 (11), 2300175.
6. Tan, L.; Yu, J.; Wang, H.; Gao, H.; Liu, X.; Wang, L.; She, X.; Zhan, T., Controllable synthesis and phase-dependent catalytic performance of dual-phase nickel selenides on Ni foam for overall water splitting. Applied Catalysis B: Environmental 2022, 303, 120915.
7. Deng, J.; Wang, Z.; Yang, H.; Jian, R.; Zhang, Y.; Xia, P.; Liu, W.; Fontaine, O.; Zhu, Y.; Li, L.; Chen, S., Superfast hydrous-molten salt erosion to fabricate large-size self-supported electrodes for industrial-level current OER. Chemical Engineering Journal 2024, 482, 148887.
8. Yue, C.; Zhang, X.; Yin, J.; Zhou, H.; Liu, K.; Liu, X., Highly efficient FeS2@ FeOOH core-shell water oxidation electrocatalyst formed by surface reconstruction

of FeS2 microspheres supported on Ni foam. Appl. Catal. B Environ 2023, 339, 123171.

9. Luo, F.; Liu, W.; Liu, Y.; Yu, P.; Jiang, X.; Chen, S., Rational modulation of interfacial electronic structure in Ni3S2/NiO pn heterojunction for efficient alkaline oxygen evolution. Chem. Eng. J 2023, 475, 146140.
10. Cai, H.; He, S.; Yang, H.; Huang, Q.; Luo, F.; Hu, Q.; Zhang, X.; He, C., Highly Exposed Ultra-Small High-Entropy Sulfides with d-p Orbital Hybridization for Efficient Oxygen Evolution. Adv.Mater 2025, 2508610.
11. Liu, Q. Q.; Huang, J. F.; Yang, D.; Feng, Y. Q.; Li, G.; Zhang, X.; Zhang, Y.; Xu, G. T.; Feng, L. L., Formation of porous NiCoV-LTH nanosheet arrays by in situ etching of nickel foam for the hydrogen evolution reaction at large current density. Dalton Transactions 2021, 50 (1), 72-75.
12. Liu, H. B.; Huang, R.; Chen, W. X.; Zhang, Y. W.; Wang, M. M.; Hu, Y. J.; Zhou, Y. M.; Song, Y. C., Porous 2D cobalt–nickel phosphide triangular nanowall architecture assembled by 3D microsphere for enhanced overall water splitting. Appl. Surf. Sci. 2021, 569, 150762.
13. Guo, X.; Song, E.; Zhao, W.; Xu, S.; Zhao, W.; Lei, Y.; Fang, Y.; Liu, J.; Huang, F., Charge self-regulation in 1T'"-MoS2 structure with rich S vacancies for enhanced hydrogen evolution activity. Nat. Commun 2022, 13 (1), 5954.
14. Yao, Y.; Zhu, Y.; Pan, C.; Wang, C.; Hu, S.; Xiao, W.; Chi, X.; Fang, Y.; Yang, J.; Deng, H., Interfacial sp C–O–Mo hybridization originated high-current density hydrogen evolution. Journal of the American Chemical Society 2021, 143 (23), 8720-8730.
15. Wang, X.; Xu, L.; Li, C.; Zhang, C.; Yao, H.; Xu, R.; Cui, P.; Zheng, X.; Gu, M.; Lee, J., Developing a class of dual atom materials for multifunctional catalytic reactions. Nat. Commun 2023, 14 (1), 7210.
16. Kim, C.; Kim, S. H.; Lee, S.; Kwon, I.; Kim, S.; Seok, C.; Park, Y. S.; Kim, Y., Boosting overall water splitting by incorporating sulfur into NiFe (oxy) hydroxide. J. Energy Chem 2022, 64, 364-371.
17. Ibraheem, S.; Li, X.; Shah, S. S. A.; Najam, T.; Yasin, G.; Iqbal, R.;

Hussain, S.; Ding, W.; Shahzad, F., Tellurium triggered formation of Te/Fe-NiOOH nanocubes as an efficient bifunctional electrocatalyst for overall water splitting. ACS Applied Materials & Interfaces 2021, 13 (9), 10972-10978.

18. Dong, J.; Wang, Y.; Jiang, Q.; Nan, Z.-A.; Fan, F. R.; Tian, Z.-Q., Charged droplet-driven fast formation of nickel–iron (oxy) hydroxides with rich oxygen defects for boosting overall water splitting. J. Mater 2021, 9 (35), 20058-20067.
19. Zhang, W.; Jiang, X.; Dong, Z. M.; Wang, J.; Zhang, N.; Liu, J.; Xu, G. R.; Wang, L., Porous Pd/NiFeOx nanosheets enhance the pH-universal overall water splitting. Adv. Funct. Mater 2021, 31 (51), 2107181.
20. Wang, S.; Ning, X.; Cao, Y.; Chen, R.; Lu, Z.; Hu, J.; Xie, J.; Hao, A., Construction of an advanced NiFe-LDH/MoS2–Ni3S2/NF heterostructure catalyst toward efficient electrocatalytic overall water splitting. Inorg. Chem. 2023, 62 (16), 6428-6438.
21. Kresse, G.; Hafner, J., Ab initio molecular dynamics for liquid metals. Physical Review B 1993, 47 (1), 558-561.
22. Kresse, G.; Hafner, J., Ab initio molecular-dynamics simulation of the liquid-metal--amorphous-semiconductor transition in germanium. Physical Review B 1994, 49 (20), 14251-14269.
23. Perdew, J. P.; Burke, K.; Ernzerhof, M., Generalized Gradient Approximation Made Simple. Physical Review Letters 1996, 77 (18), 3865-3868.
24. Kresse, G.; Joubert, D., From ultrasoft pseudopotentials to the projector augmented-wave method. Physical Review B 1999, 59 (3), 1758-1775.
25. Grimme, S.; Antony, J.; Ehrlich, S.; Krieg, H., A consistent and accurate ab initio parametrization of density functional dispersion correction (DFT-D) for the 94 elements H-Pu. The Journal of Chemical Physics 2010, 132 (15).